Optimizing fPET-FDG

Thomas M. Morin

Tufts University

Abstract

Recent work by Villien, et al. presented the development of a new functional brain imaging method known as fPET-FDG (2014). With this method, it is possible to observe repeated task-specific changes in cerebral glucose metabolism during a single dynamic PET scan. Previously, the method has been limited to detecting these changes only at late time-points, 20-30 minutes after the start of a scan.

We hypothesized that with an improved protocol for the administration of the 2-[^{18}F]-fluoro-deoxyglucose (FDG) radiotracer, we could detect task-specific changes in FDG signal at earlier time points than was previously possible. Simulations suggested that in order to detect these changes, we would require a specialized general linear model (GLM), different from that used in previous fPET-FDG studies. Using the new GLM, our study demonstrated the successful detection of these task-specific signal changes at early time points in one subject. Further work is needed to validate this model and to replicate it in other subjects.

Future optimization of the fPET-FDG methodology could allow us to examine dynamic changes in glucose metabolism associated with working memory, attention, and other areas of cognition. The fPET-FDG method could be especially useful in detecting real-time task-specific metabolic changes associated with various diseases such as diabetes.

Optimizing fPET-FDG

Over the last half century, the steady improvement of neuroimaging with positron emission tomography (PET) has made it a fundamental tool in the study of the human mind and brain. It has become common for most major research universities and hospitals to possess the necessary infrastructure to study brain function, whether it is through PET or a number of other technologies such as functional magnetic resonance imaging (fMRI) (Jones & Rabiner, 2012). Although fMRI is currently the preferred tool for functional brain imaging among neuroscientists and psychologists, some of the key foundational studies that formed the bedrock of this field were conducted with PET neuroimaging (Jones & Rabiner, 2012).

PET is a versatile tool that can be adapted to investigate a range of topics related to brain chemistry and function. Some of the most prominent applications of PET imaging to brain research include studies of endogenous neurotransmitter release, the binding characteristics of potential neuro-pharmaceuticals, and enzyme activity (Placzek, Zhao, Wey, Morin, & Hooker, 2016). More recently, PET studies have even sought to investigate epigenetic changes in the human brain (Wey et al., 2016). In addition to drug-discovery ventures and the search for disease biomarkers, PET neuroimaging technologies are also commonly used to answer questions about brain function.

Origins of Functional PET Imaging

Some of the first experiments to study functional activity in the brain used water labeled with oxygen-15 ($[^{15}O]H_2O$) as a radiotracer to measure changes cerebral blood flow (CBF). By measuring regional changes in CBF with $[^{15}O]H_2O$, early studies successfully mapped the visual cortex (Endo et al., 1997; Fox et al., 1986), identified brain areas associated with lexical processing (Petersen, Fox, Posner, Mintun, & Raichle, 1989), pinpointed brain regions important

in attention (Corbetta, Miezin, Dobmeyer, Shulman, & Petersen, 1990), and identified the "what" and "where" pathways associated with visual recognition (Haxby et al., 1991).

These studies all utilized the same experimental paradigm: acquire one PET image while the subject is at rest as a control, and another image while the subject is completing a cognitive task. When the control image is subtracted from the task image, we are left with task-associated changes in PET signal (Fox, Mintun, Reiman, & Raichle, 1988). This method is referred to as the double-bolus method because it requires two-separate "bolus" injections of the radiotracer. Functional PET imaging methods of this sort served as part of the inspiration for the development of fMRI (Belliveau et al., 1991; Kwong et al., 1992). Without the need for an exogenous contrast or radioactive material, fMRI quickly gained popularity as a more user-friendly and cost-effective alternative to PET. Moreover, with the development of echo planar imaging (EPI), fMRI's temporal resolution (now on the order of seconds) quickly surpassed that of PET (now on the order of minutes). Today (April 4, 2017) a PubMed search for "functional MRI" produces 448,880 results, while a search for "functional PET" yields only 8,575.

Early researchers who used $[^{15}O]H_2O$ to measure functional brain activity faced several challenges. Because the $[^{15}O]H_2O$ radiotracer decays rather quickly (^{15}O has a half-life of only 122 seconds), these early PET studies required careful planning and advanced resources. Studies with $[^{15}O]H_2O$ require subjects to undergo several separate scans in order to repeat the task multiple times; once the radioactivity runs out from an initial dose of radiotracer, another dose must be administered. Because $[^{15}O]H_2O$ has a particularly short half-life, an on-site cyclotron is also required to synthesize the tracer.

Functional Brain Imaging with FDG

Another radiotracer that is commonly used in functional neuroimaging is 2-[^{18}F]-fluoro-deoxyglucose (FDG). As an analogue for glucose, FDG was developed to investigate the brain's energy use through the quantification of cerebral glucose metabolism (Reivich et al., 1979). In the years since its first use in humans, FDG has helped scientists draw conclusions about changes in glucose metabolism that are associated with a wide array of mental disorders and brain diseases (for examples, see: Alexander, Chen, Pietrini, Rapoport, & Reiman, 2002; Paulesu et al., 1996).

FDG's continued utility and success as a radiotracer stems from its longer half-life of 109.7 minutes and its optimized synthesis (Cole, Stewart, Littich, Hoareau, & Scott, 2014). Because it can be synthesized off-site and then delivered to the PET scanning bay, FDG is a more user-friendly radiotracer than [^{15}O]H$_2$O. A single dose of FDG administered intravenously can provide enough PET signal for longer dynamic scans of up to 90 minutes or more.

FDG studies of *functional* brain imaging have traditionally made use of the double-bolus experimental design. Double-bolus experiments with FDG have allowed researchers to track changes in cerebral metabolic rate of glucose (CMR$_{glu}$) associated with various cognitive/behavioral tasks and even pharmacological challenges (Hampson, Porrino, Opris, Stanford, & Deadwyler, 2011; Iozzo, Guiducci, Guzzardi, & Pagotto, 2012; Yehuda et al., 2009). However, the double bolus method suffers from several limitations. The static images captured by the double bolus method are only able to track changes that occur between two separate scans. These scans are often days, weeks, or even moths apart. This limits the amount of control experimenters have over external factors such as sleep, caffeine or food intake, and presents logistical issues when it comes time to co-register the two images (Villien, et al., 2014).

Recently, two studies have proposed and validated a new method for functional PET imaging with FDG that aims to overcome the limitations of the double bolus method (Hahn et al., 2016; Villien et al., 2014). Known as fPET-FDG, the method allows subjects to be presented with multiple cognitive tasks over the course of a single scan, in an experimental design similar to that which is commonly used in fMRI studies. The initial paper demonstrated that the fPET-FDG method could successfully detect significant changes in FDG signal in area V1 of the visual cortex during presentation of a visual stimulus (Villien, et al., 2014). Additionally, fPET-FDG was sensitive enough to detect FDG signal changes in just one hemisphere of the brain when the stimulus was presented on one half of the subject's visual field. Further work by Hahn, et al. revealed that the method was even sensitive enough to detect changes in FDG signal in the motor cortex during a finger-tapping task (2016). Both studies have shown that task-specific changes in FDG signal are associated with changes the cerebral metabolic rate of glucose (CMR_{glu}), and that these changes in CMR_{glu} can be quantified (Hahn, et al., 2016; Villien, et al., 2014).

Kinetic Modeling of FDG

The main goal of the fPET-FDG method is to examine how task-specific glucose metabolism differs across brain regions. However, the raw signal detected by the PET scanner is composed of more than just glucose that is being metabolized. The PET scanner will detect radioactivity wherever the FDG tracer is present, whether it is in the blood or inside of cells. Figure 1a shows three different configurations of FDG that contribute to the overall observed PET signal: (1) FDG in blood plasma, (2) FDG inside of cells, and (3) phosphorylated FDG inside of cells (figure adapted from Kelloff et al., 2005). Since fPET-FDG is concerned with glucose metabolism, we are most interested in the phosphorylated FDG; phosphorylation is the first step in the cellular metabolic process of glycolysis.

With kinetic modeling, we can parse out the portion of the overall signal that is contributed by phosphorylated FDG. The standard way of doing this is to construct a two-tissue compartment (2-TC) model (Figure 1b) (Bertoldo et al., 1998; Kelloff, 2005). The 2-TC model is built by considering each of the three different configurations of FDG as a single compartment. The FDG in blood plasma is summarized by the plasma compartment C_p. The two "tissue" compartments, C_1 and C_2, represent intracellular FDG and phosphorylated FDG respectively. We also define four rate-constants, $K_1 - k_4$, to describe the rate at which the radiotracer moves between each compartment. K_1 is the rate of FDG-influx as it is carried from the blood stream, across the cell membrane, and into the cell by the Glut-1 transport protein. k_2 is the rate of FDG-efflux out of the cell and back into the bloodstream. k_3 is the rate at which FDG is phosphorylated by the enzyme hexokinase, and k_4 is the rate at which FDG is dephosphorylated by the enzyme Glucose-6-Phosphotase. When modeling FDG, k_4 is often set to zero or close to zero because dephosphorylation by Glucose-6-Phosphotase occurs at a very slow rate in cerebral tissues (Bertoldo et al., 1998; Reivich et al., 1979; Sokoloff et al., 1977).

With a compartment model in place, we can define a system of differential equations to describe the rate of change of FDG concentration in each of the two tissue-compartments over time (Figure 1c). As input, the system of differential equations requires (1) specific values for each of the rate constants $k_1 - k_4$, and (2) a function that represents the concentration FDG in the plasma compartment, defined as $C_p(t)$. The rate constants $k_1 - k_4$ will differ depending on the tissue we are examining and the plasma input function will differ depending on how the radiotracer is injected. With the proper input, the system of differential equations can be solved and the concentration of FDG in each of the three compartments over time can be plotted as a time-activity curve (TAC).

Figure 1d shows TACs for each of the compartments in the 2-TC model when FDG is constantly infused for 60 minutes, and the rate constants are set to specific values. It is worth noting that the values chosen for rate constants can vary slightly between studies. In our simulations, we chose the values: $K_1 = 0.1$, $k_2 = 0.2$, $k_3 = 0.11$, and $k_4 = 0.001$ (O'Sullivan et al., 2010; Reivich et al., 1985). The red line represents the plasma input function $C_p(t)$ which we provided to the model. The dashed blue and solid black lines represent the concentration of FDG over time in compartments C_1 and C_2 respectively. The purple curve represents the observed PET signal in brain tissue (a sum of the signals in C_1 and C_2).

Motivation

Despite its numerous successes, the fPET-FDG method faces several limitations that require further experimentation. Because the two initial studies were pilot studies, researchers used visual and finger-tapping tasks that were 5-10 minutes in duration (Hahn, et al., 2016; Villien, et al., 2014). By using such lengthy tasks, researchers could practically guarantee that they would detect any and all task-related signal changes. While it is believed that a better temporal resolution (tasks that are shorter than 5-10 minutes) may be possible, it has never been tested before. Additionally, the original fPET-FDG method requires an initial "equilibration period" of 20-30 minutes before participants can be tasked. This waiting time is required to ensure that an adequate amount of the radiotracer accumulates in the brain and is available for metabolism (Villien, et al., 2014).

The requirement of an "equilibration period" stems from the way the FDG radiotracer was administered to participants in the original fPET-FDG studies. These studies utilized a constant infusion protocol by which an infusion pump administered the radiotracer intravenously at a constant rate throughout the entire scan. In contrast to a more traditional bolus injection, the

constant infusion paradigm allows researchers to better quantify changes in glucose metabolism. When the radiotracer is constantly infused, FDG signal in the brain rises at a predictable and constant rate, but only after the initial equilibration period – it takes some time for the signal in tissue to "accelerate" to its full rate.

PET experiments with other radiotracers such as [^{11}C]racolpride have utilized a novel injection protocol, known as a bolus plus continuous infusion (B/I) protocol, that is capable of shortening the equilibration period at the beginning of a scan (Carson et al., 1993). With the B/I method, a partial dose of the radiotracer is administered as an initial bolus injection at the start of the scan. The remaining portion of the dose is then constantly infused throughout the remainder of the scan.

Hypothesis

In this study, we set out to improve the fPET-FDG method with an optimized tracer injection protocol. We believed that a more efficient tracer injection protocol would shorten the necessary equilibration period, allowing us to present subjects with their first cognitive task at earlier time points in an fPET-FDG scan. From a series of simulations, we predicted that a B/I protocol would allow us to detect task-specific changes in FDG signal as early as ten minutes after the start of the scan. To account for the B/I protocol, we also proposed an updated mathematical model for predicting task-specific signal changes in the analysis of fPET-FDG images.

Methods

Participants

Four participants (4 M, 0 F) between 18 and 65 years of age ($M = 29.3$, $SD = 12.6$) underwent the scanning procedure outlined below. One participant exited the scanner 10 minutes

early because he had to use the bathroom. The other three participants completed the entire 60-minute scan. Upon successful completion of the study, participants were compensated $125 for their time. The study was approved by the Partners Healthcare Institutional Review Board. All participants were screened prior to their visit to ensure that they met basic exclusion criteria and that it was safe for them to undergo an MR-PET scan. Prior to beginning the study, participants gave written informed consent.

Experimental Procedure

Participants were asked to fast for at least four hours before completing the study, so that we could take accurate blood-glucose-level measurements. The study was conducted at the Antinhola A. Martinos Center for Biomedical Imaging at Massachusetts General Hospital in Charlestown, MA, USA. Just before entering the scanning bay, a blood sample was collected from participants to determine baseline blood glucose levels. Throughout the scan, additional blood samples were collected by a trained technician at ten-minute intervals.

During the scan, visual stimuli were projected from behind the scanner onto a small mirror mounted on the head-coil. Participants were instructed to direct their gaze at a fixation cross on the screen for the duration of the scan. The 60-minute scan was divided into four 15-minute blocks, each consisting of a 10-minute rest period followed by a 5-minute task period. During the rest periods, a small black fixation cross was displayed on a blank white screen. During task periods, a black and white checkerboard pattern was flashed on the screen with a frequency of 8 Hz (Polimeni, Fischl, Greve, & Wald, 2010). Stimuli were created and presented using PsychoPy2 software (Peirce, 2007, 2008). See Figure 2 for a flow chart of the experimental procedure.

MR/PET Imaging

Simultaneous MRI and PET images were acquired on a 3-T TIM MAGNETOM Trio MR scanner (Siemen's Healthcare, Inc.) with an MR-compatible BrainPET insert (Siemens). Scanning parameters were identical to those outlined in the previous study by Villien, et al. (2014), with the exception that our scan lasted only 60-minutes. MRI acquisition consisted of a high-resolution T1-weighted structural scan taken before the injection of FDG, and functional imaging throughout the scan. In this paper, we do not discuss the fMRI imaging.

FDG in saline was administered in a B/I protocol (Carson et al., 1993). The FDG dose was split in half so that 3mCi was injected intravenously in the initial bolus and 3mCi was constantly infused intravenously throughout the 60-minute scan. This ratio was chosen after conducting computer simulations of various injection protocols (see below). A trained technician at the beginning of the scan administered the initial bolus dose manually. A Medrad® Spectra Solaris syringe pump was used to administer the subsequent infused dose. PET data were reconstructed using an in-house software tool implemented in MATLAB (Natick, MA) (Chonde, Izquierdo-Garcia, Chen, Bowen, & Catana, 2014). PET data were binned into 60 one-minute frames and reconstructed into 76 slices of dimension 128 x 128 voxels, with an isotropic voxel size of 2.5mm^3.

Injection Protocol Simulations

To determine the optimal B/I protocol for this study, we conducted several computer simulations before scanning. All simulations were conducted with in-house software written by the author in MATLAB (Natick, MA). While previous fPET-FDG studies utilized a constant-infusion protocol (Hahn et al., 2016; Villien et al., 2014), we hypothesized that a B/I protocol might allow us to present the visual stimulus earlier in the scan, instead of waiting the standard

20 - 30 minute long equilibration period. With a B/I protocol, the experimenter must choose the ratio of bolus-administered tracer to infusion-administered tracer. This ratio is summarized by the parameter K_{bol} (Carson et al., 1993). The K_{bol} for a particular B/I protocol is equal to the magnitude of the bolus-administered dose, measured in minutes of infusion. For example, if K_{bol} = 30 minutes, then the dose of the initial bolus is equivalent to the dose that would be infused over 30-minutes of scan-time.

To predict the optimal K_{bol} for our study, we simulated a whole-brain-averaged time activity curve (TAC) for several different values of K_{bol} (see Figure 3). For the simulations, we used a method proposed by Carson, et al. (1993) that requires as input: (1) a K_{bol} parameter and (2) a TAC from a standard bolus injection paradigm. As output, the method produces the expected TAC for a B/I protocol.

The TAC from a standard Bolus injection was simulated using a 2-Tissue Compartment Model described by the following system of differential equations (Normandin & Morris, 2008; Wernick & Aarsvold, 2004):

$$\frac{dC_1(t)}{dt} = k_1 C_p(t) - (k_2 + k_3)C_1(t) + k_4 C_2(t) \tag{1}$$

$$\frac{dC_2(t)}{dt} = k_3 C_2(t) - k_4 C_2(t) \tag{2}$$

where $C_p(t)$ is the blood plasma input function, $C_1(t)$ is the intracellular FDG compartment, $C_2(t)$ is the phosphorylated FDG compartment, and k_1 through k_4 are the kinetic rate constants unique to the tracer. For FDG, we chose rate constants of $K_1 = 0.1$, $k_2 = 0.2$, $k_3 = 0.11$, and $k_4 = 0.001$ (O'Sullivan et al., 2010; Reivich et al., 1985). k_4 was intentionally chosen as a value close to zero, because FDG demonstrates irreversible binding properties with limited washout (Bertoldo et al., 1998; Reivich et al., 1979; Sokoloff et al., 1977). The plasma input function

$C_p(t)$ was generated the following model in Equation 3 (Feng, Huang, & Wang, 1993; Normandin & Morris, 2008):

$$C_p(t) = (\beta_1 - \beta_2 - \beta_3)e^{-\kappa_1 t} + \beta_2 e^{-\kappa_2 t} + \beta_3 e^{-\kappa_3 t} \tag{3}$$

Our implementation of the plasma input function used values $\beta_1 = 12\text{nM} \cdot \text{min}^{-1}$, $\beta_2 = 1.8\text{nM}$, $\beta_3 = 0.45\text{nM}$, $\kappa_1 = 4\text{min}^{-1}$, $\kappa_2 = 0.5\text{min}^{-1}$, and $\kappa_3 = 0.008\text{min}^{-1}$ (Feng et al., 1993). Using these constants, we generated a 60-minute plasma curve with activity values generated at 30-second intervals. The plasma curve was then used as input in the 2-TC model. The 2-TC model was solved using the ordinary differential equations solver in MATLAB. The resulting tissue TAC was used to simulate B/I TACs for various values of K_{bol} using Equation 4. In Appendix 1, we outline how this equation was derived form Carson, et al. (1993).

$$TAC_{BI}(t) = R_{bolus}f(t) + R_{infusion}\frac{\int_0^t f(\tau)d\tau}{T} \tag{4}$$

where $R_{bolus} = \frac{K_{bol}}{K_{bol}+T}$, $R_{infusion} = 1 - R_{bolus}$, $f(t)$ is the tissue TAC form a bolus protocol generated with the 2TC model, and T is the duration of the scan in minutes. Integrals were solved using trapezoidal numerical integration.

Figure 3 shows the expected average TACs for the whole-brain given different values of K_{bol}. From this simulation, we sought the K_{bol} that brought the TAC to an approximately linear slope most efficiently. We chose a K_{bol} of 60 minutes because the simulation showed a rapid transition to a linear slope, achieving this after just 10 minutes.

Determining how to split the tracer dose between bolus and infusion when $K_{bol} = 60$ min. is a simple calculation for a 60-minute scan. With a $K_{bol} = 60$ min. for a 60-minute scan, we split the 6mCi radiotracer dose in half so that 3mCi was injected during the initial bolus, and the other 3mCi was constantly infused throughout the scan.

fPET Analysis Overview

Each subject's PET data was processed using a registration and analysis pipeline similar to those used by Villien, et al. (2014). First, a mean volume of each subject's dynamic PET image was calculated. This mean volume was co-registered to a standard low-resolution T1-weighted image (62 slices of 50 x 50 voxels with dimension 2.98mm x 3.03mm x 2.96mm) using an affine linear transformation (12 degrees of freedom) implemented by the Jip Analysis Toolkit (© The General Hospital Corporation). The resulting transformation matrix was then applied to the original dynamic PET images to register them to the low-resolution image. Co-registered dynamic PET images were then smoothed with a 12mm Gaussian kernel.

A general linear model (GLM) was fitted to each voxel's TAC in the smoothed images to produce T-statistic maps using the Jip Analysis Toolkit (© The General Hospital Corporation). Statistical maps were corrected for multiple comparisons and thresholded using random field theory. Statistical maps for each subject were brain-extracted, registered to anatomical space using a boundary-based registration, and projected onto a surface of the corresponding anatomical images using FreeSurfer software (Fischl, 2012). The resulting activation maps, with a threshold of T > 5.0 are displayed in Figure 7. Activation maps were not created for Subject 2 because he exhibited a high degree of motion (> 5mm) during the scan.

General Linear Model

Like in previous fPET studies, a GLM was fitted to each voxel's TAC to determine if there was a significant change in FDG signal during the task period as compared to the rest period (Hahn et al., 2016; Villien et al., 2014).

$$Y = \beta * X + \varepsilon$$

$$TAC = \beta_{baseline} * regressor_{baseline} + \beta_{task} * regressor_{task} + \varepsilon \qquad \textbf{(5)}$$

The GLM included two regressors (see Equation 5). The first was a baseline regressor defined as a quadratic fit of the voxel's TAC. The second regressor was based on the visual stimulus paradigm. The model we chose for the task regressor differs from that used in previous fPET-FDG studies because of our use of the B/I protocol.

Previous fPET-FDG studies have defined the task regressor as a series of "ramp" functions to model the stimulus paradigm. To create the "ramp" functions, we first would create an "on-off" time-series vector, where 0 (off) is assigned to time points during the resting periods, and a 1 (on) is assigned to time points during the task periods. The "ramps" would then be created by taking the integral of the "on-off" vector. The resulting regressor has a shape where the slope increases at a constant rate during the task periods, but stays flat during rest periods.

This model worked for previous studies because a constant infusion injection paradigm was used, and all task periods occurred at late time points (after the first 25 minutes). Simulations reveal that the linearity of a tissue TAC at late time points in an fPET-FDG scan guarantees that for any two identical tasks, increases in FDG signal would be identical. This ensures that corresponding "ramps" in a task-regressor for the GLM could also have identical slopes.

Attempts to use this type of regressor in the current study revealed that it did not effectively model the data. Simulations suggested that when using a B/I protocol with a task-period early in the scan, increases in FDG signal were not identical at early and late time points. At earlier time-points, the influx of FDG in the plasma compartment is much faster due to the combined influence of both the initial bolus input and the constant infusion input. This results in a much sharper task-specific increase in FDG signal at early time points compared to task-specific changes at late time points.

An appropriate task regressor for our study needed to account for these variations in task-specific changes. To generate this regressor, we first simulated the expected tissue TAC for our study. Using a 2-TC model with a B/I plasma input function (Kbol = 60 min.), we generated TACs for each compartment. To account for changes in glucose metabolism during a task, we doubled the value of k_3 (the rate constant associated with glucose metabolism) during each of the five-minute task periods. To compute the "on-off" vector, we took the derivative of the TAC from the metabolized FDG compartment (C_2), and set all time-points during the resting-periods to zero. The resulting "on-off" vector shows varying degrees of "on" that correspond to the varying changes in the slope of the TAC for C_2 during task-periods. The final task regressor was created by integrating the "on-off" vector. Regressors for various values of K_{bol} are displayed in Figure 8.

Results

We successfully acquired dynamic PET data, blood glucose measures, and venous plasma samples from all four participants with the following minor exceptions: Subject 1 ended the scan 10 minutes early because he had to use the bathroom. Because of this, we did not acquire PET images or blood samples for subject 1 after the 50-minute mark. Additionally, due to experimenter error, we were not able to quantify plasma activity levels for subject 3 at the 10-minute time point.

While all four subjects did fall within the height and weight ranges necessary to safely undergo an MR-PET scan, body mass index (BMI) calculations indicated that subject 1 (*BMI* = $31.5 kg/m^2$) was obese, and that subject 2 (*BMI* = $25.9 kg/m^2$) and subject 3 (*BMI* = $28.9 kg/m^2$) were overweight. Only subject 4 (*BMI* = $23.1 kg/m^2$) was of normal weight.

Additionally, subject 1 had an abnormally high baseline fasting plasma glucose (FPG) level of 102mg/dL. The next FPG measure form subject 1 at the 30-minute mark returned to within the normal range (*FPG* = 86mg/dL). While the other subjects did not exhibit abnormally high baseline FPG measures, subjects 2 and 3 did exhibit FPG levels on the upper-end of the normal range, 90 mg/dL and 99 mg/dL respectively. For context, the American Diabetes Association classifies normal FPG levels as < 100 mg/dL, and diabetic levels as > 125 mg/dL. Patients with FPG levels between 100 − 125 mg/dL, are classified as having impaired glucose tolerance and being pre-diabetic. Our study's protocol allowed participants to complete the study as long as they did not have a history of diabetes.

K_{bol} Selection

After simulating the tissue TACs resulting from a range of K_{bol} values, we chose to fix K_{bol} at 60 min. for this study. Figure 3 shows simulated tissue TACs given values of K_{bol} ranging from 0 to 100 with increments of 20. When K_{bol} = 0 min., the B/I protocol is actually just a constant infusion protocol, since there is no initial bolus. The corresponding tissue TAC is therefore identical to the expected tissue TAC from a constant infusion protocol. From this simulation, we sought to determine the value of K_{bol} that would bring the TAC to a linear slope most efficiently, thereby minimizing the necessary equilibration period. For all simulated values of K_{bol} > 0 min., the TACs reached a linear slope more quickly than what is expected from a constant infusion paradigm. For our study, we chose a K_{bol} = 60 minutes because the simulation showed a rapid transition to a linear slope, achieving this after just 10 minutes. While a higher K_{bol} may have reached a linear slope even faster, any potential improvement seemed marginal. Additionally, since we are limited to a fixed amount of radioactivity that can be safely injected into human participants, increasing the K_{bol} would require us to administer less radiotracer during

the constant-infusion portion of the study. Since the radiotracer decays throughout the study, it was in our best interest to choose the lowest possible effective K_{bol}, ensuring that an adequate amount of radiotracer would be allocated for the constant infusion portion of the B/I protocol.

Venous plasma TACs suggest that the simulations were correct and that 60 min. was a suitable value for K_{bol} in this study. Radioactivity in venous plasma was quantified at 10-minute intervals during the scan. Normalized measures for each subject, along with an average curve for all subjects are plotted in Figure 4. Visual inspection of the average curve shows that after 10 minutes, a relatively constant value is maintained. This confirms that equilibrium was reached in the plasma compartment early in the scan, suggesting that the equilibration period was effectively minimized.

GLM Fit

Figure 5 shows the GLM fit for subject 4. The time activity curves shown were extracted from two *a priori* regions of interest (ROIs) of identical shape and size. One ROI was from a portion of the frontal lobe, and the other was from a portion in the occipital lobe. ROIs were manually generated and TACs were extracted using PMOD (version 3.310, PMOD Technologies Ltd., Zürich, Switzerland). The TACs from these ROIs show increased CMR_{glu} in the occipital ROI compared to the frontal ROI throughout the entire scan. Additionally, the overall GLM fit shows that while changes in occipital TAC slope are quite obvious during the first task-period, subsequent task-specific changes in slope are much smaller in magnitude, as was predicted by our simulations. Figure 5b. shows the result of subtracting out the baseline quadratic regressor of the GLM from the occipital TAC. (For demonstration, we defined the baseline regressor as a quadratic fit of the frontal ROI). A fit of the task-regressor to the baseline-subtracted occipital data is also quite good, although it is noticeably noisy.

fPET-FDG Activations Maps

Due to a high degree of motion during the scan (> 5mm), Subject 2 was excluded from fPET-FDG activation analysis. Figure 6 shows both the traditional and newly designed task regressors used in this analysis, and the associated statistical maps, all for subject 4. In figures 6 and 7, statistical maps were corrected for multiple comparisons using random field theory and thresholded at T > 5.0. The traditional task regressor, used in previous fPET-FDG studies, predicts that each task-period will result in identical increases in FDG signal. The newly designed task regressor, optimized for the B/I protocol, predicts that *earlier* task periods would result in larger observed increases in FDG signal than *later* task periods. In line with simulations, the use of a GLM with the traditional task regressor did not yield any significant task-associated activation clusters in any subjects (see Figure 6a for an example in Subject 4). However, when using the newly designed regressor, GLM analysis did yield clusters of activation in Subject 4 (see Figure 6b). Clusters of activated voxels appeared bilaterally in a region of the subject's occipital lobe that qualitatively aligns with visual area V1 and matches previously reported fPET-FDG results (Villien, et al., 2014).

Figure 7 shows statistical maps of fPET-FDG signal in all subjects. These maps were created with a GLM analysis that used the newly designed task regressor. Subjects 1 and 3 did not show any significant clusters of activation in these maps. As discussed above, subject 4 exhibited significant clusters of activation bilaterally in the occipital lobe.

Discussion

We hypothesized that with an improved protocol for the administration of the FDG radiotracer, we would be able to detect task-specific changes in FDG signal at earlier time points than was previously possible with fPET-FDG. Specifically, we predicted that using a B/I

protocol (K_{bol} = 60 min.) would allow us to detect task-specific changes in FDG signal as early as 10-minutes after the start of a scan. Simulations suggested that in order to detect these changes, we would require a specialized general linear model, different from that used in previous fPET-FDG studies. Our study demonstrated that in subject 4, the detection of these task-specific signal changes was possible with a newly designed GLM. In Subjects 1 and 3, we were unable to detect these changes. Subject 2 was excluded from the analysis due to significant head motion (> 5mm).

A closer look at subjects 1 and 3 suggests several confounding variables that may be limiting our ability to detect changes in their rate of cerebral glucose metabolism. The baseline fasting plasma glucose (FPG) level of subject 1 was above the normal range (*FPG* = 102 mg/dL). This subject's FPG measure likely falls within a typical margin of error for the normal range, which is capped at 100 mg/dL. However, a high FPG measure could also indicate that the subject ate prior to the scan or that the subject was pre-diabetic. Either of these circumstances could result in dynamic changes in glucose metabolism that affect FDG signal. Moreover, according to body mass index (BMI) cutoffs set by the Centers for Disease Control and Prevention, subject 1 was obese (*BMI* = 31.5 kg/m^2) and subject 3 was overweight (*BMI* = 28.9 kg/m^2) (Centers for Disease Control and Prevention, 2015).

Notably, the three participants in the first fPET-FDG study by Villien, et al. were all of normal height and weight (N. Zürcher, personal communication, April 7, 2017). Because of this there is no way to know whether weight is a confounding variable in the current study. Increased body weight of a patient or subject has been associated with increased logistical challenges during FDG PET scans (Botkin & Osman, 2007). Previous work also indicates that baseline glucose metabolism may differ in overweight and obese populations (Iozzo et al., 2012; Volkow

et al., 2009; Wang et al., 2002). Studies have predicted both increased and decreased resting *baseline* glucose metabolism in numerous brain regions. Currently, it is unknown whether increased body-weight is associated with *dynamic* changes in cerebral glucose metabolism, and further experimentation is necessary.

In subject 4, we successfully detected task-specific changes in glucose metabolism. Like the subjects in the first fPET-FDG study, this subject was of normal healthy weight (*BMI* = 23.1 kg/m^2), and had a normal healthy baseline glucose level (*FPG* = 77 mg/dL). It is also worth noting that subject 4 was recruited to participate in the study because he was a friend of the author. Subject 4 was therefore highly motivated to complete the study and to follow instructions closely. For example, it is unknown whether subjects 1 and 3 may have fallen asleep in the scanner or closed their eyes during the presentation of the flashing checkerboard stimulus.

Even in the absence of all confounds, it is possible that the study design itself limited our ability to detect task-specific changes in FDG signal. Upon close visual inspection, the activation clusters in subject 4 are slightly weaker than the activations reported by Villien (2014). We believe that when choosing a tracer administration protocol, there may be an early/late time-point trade-off. Although the B/I protocol allows us to detect signal changes at early time points, it may also hinder our ability to detect signal changes at later time points. The newly designed GLM task-regressor for this study predicts that with a B/I protocol, task-specific changes in FDG signal will be greater at early time points than at late time points. Figure 5b shows that in subject 4, the model's predictions are correct. We suspect that small changes in FDG signal are especially difficult to detect at late time points because as the radiotracer decays throughout the scan, statistical noise tends to increase (Teymurazyan, Riauka, Jans, & Robinson, 2013).

Figure 8 shows a range of task-regressors for a range of B/I protocols with various values of K_{bol}. As K_{bol} increases, the early/late time-point trade off that we have described above becomes even more pronounced. For instance, when K_{bol} = 75 min., the predicted FDG signal change from the first stimulus is more than four times larger than the predicted FDG signal change from an identical stimulus displayed at the end of the scan. On the other end of the spectrum, a constant infusion paradigm (K_{bol} = 0 min.) predicts that all task-associated changes in FDG signal will be identical in magnitude; no matter what time the stimulus is displayed. Still, because very little radiotracer has accumulated in the brain at early time-points and in a constant infusion protocol, it may be difficult to detect task-specific changes at early time points before the equilibration period is over.

If the model presented in Figure 8 is correct, the optimal K_{bol} for an fPET-FDG study may be lower than the K_{bol} = 60 min. that we had selected for this study. For example, a K_{bol} in the range of 15-30 minutes seems to provide a decent compromise for the proposed early/late time-point trade off. Because we have only demonstrated that this model is successful in one subject and for one value of K_{bol}, further validation is needed. Future studies looking to validate this model would need to test it in multiple subjects and for a range of K_{bol} values.

With the data we have already collected, we may be able to conduct further analyses to validate the proposed model. Although subject 2 was excluded for motion, new MRI-based motion correction tools may provide us with usable dynamic PET images. This is possible only because we collected the data on a simultaneous MR/PET scanner and acquired simultaneous fMRI data. Additionally, our research group has an untouched dataset of about a dozen subjects who participated in a similar fPET-FDG experiment. While most of these subjects underwent the

standard constant infusion protocol, one subject underwent an abbreviated constant infusion protocol that a variation of the model could be tested on.

The existing dataset also contains several subjects who are overweight, but underwent the standard constant infusion protocol. fPET-FDG analysis of these subjects' data could potentially lead to some interesting conclusions about whether bodyweight influences dynamic changes in glucose metabolism.

Future analysis of the data from this study could also examine the functional MRI data that was acquired concurrently with the fPET-FDG data. Because FDG signal can be used to quantify CMR_{glu}, fPET-FDG may offer a quantifiable measure of brain activity that complements the more qualitative measures of BOLD fMRI. The manifestation of neuronal activity as BOLD signal is not completely understood. It is hypothesized that BOLD signal depends on numerous factors including blood flow, oxygen consumption, the characteristics of microvasculature, and the MR sequence used to acquire the data (Gagnon et al., 2015; Jueptner & Weiller, 1995; Pike, 2012). ASL data acquired during the second half of each scan during our study could be used to investigate the influence of CBF on CMR_{glu}. With the simultaneous MR/PET modality, it is possible that future fPET-FDG studies could shed some light on the origins of BOLD signal, particularly portions of the signal that may be linked to metabolism.

For the current study, we have also reconstructed the dynamic PET images into 30-second and 10-second bins. While this data is likely quite noisy due to decreased counts in each bin when compared to the 1-minute reconstruction, the fPET-FDG methodology would benefit immensely from an improved temporal resolution for dynamic PET. To push the temporal limits of the methodology, future studies might also attempt to shorten the length of a task period or rest period. Currently, no fPET-FDG task has been shorter than five minutes in length, and all

fPET tasks have been separated by a period of at least five minutes (Hahn, et al., 2016; Villien, et al., 2014).

Ultimately, we hope that future fPET-FDG studies utilize cognitive tasks that were originally designed for fMRI paradigms. For example, an n-back working memory task could be used to investigate dynamic changes in glucose metabolism associated with working memory. Previous work has established a link between decreased resting CMR_{glu} and decreased working memory capacity in Alzheimer's Disease (Kalpouzos et al., 2005). However, it is currently unknown what normal dynamic changes in glucose metabolism might exist in healthy subjects completing a working memory task. Numerous improvements need to be made to the fPET-FDG methodology before we can be sure that it is capable of detecting the miniscule changes in glucose metabolism that are likely associated with a working memory task. Still, the potential for this line of research exists.

In the future, fPET-FDG may also be of use to researchers and clinicians interested in performing functional brain imaging on patients with metallic implants. While metallic implants for deep brain stimulation are becoming MR-compatible with greater frequency (Zrinzo et al., 2011), something as simple as an aneurysm clip can still exclude participants from MRI experiments. Because it does not require a large magnetic field, future fPET-FDG may someday be a safe alternative to fMRI for patients with metallic implants.

The fPET-FDG method may also be of interest to clinicians interested in diseases like diabetes which involve poor control of glucose metabolism. Research has shown increased incidence of cognitive deficits in patients with poor metabolic control, such as those with diabetes (Baker et al., 2011; Ryan et al., 2006). A simultaneous fMRI/fPET-FDG study might present diabetic patients with a set of cognitive tasks and a sports drink used as a glucose

challenge. Results from a study like this might map the brain areas associated with these patients' cognitive deficits, and then see how those regions correlate with areas exhibiting poor metabolic control during the glucose challenge.

While many of the applications for fPET-FDG might seem highly imaginative and out of reach, the current study probably would have sounded just as crazy to some of the first PET researchers. The ability to measure functional changes in glucose metabolism with fPET-FDG has opened up a whole new field of possibilities for neuroimaging researchers. With further work and steady methodological improvement, the fPET-FDG methodology has the potential to enhance our understanding brain function. With fPET-FDG added to their toolkit, neuroscientists and psychologists can develop novel explanations for how the brain and mind work.

References

Alexander, G. E., Chen, K., Pietrini, P., Rapoport, S. I., & Reiman, E. M. (2002). Longitudinal PET Evaluation of Cerebral Metabolic Decline in Dementia: A Potential Outcome Measure in Alzheimer's Disease Treatment Studies. *American Journal of Psychiatry*, *159*(5), 738–745. https://doi.org/10.1176/appi.ajp.159.5.738

Baker, L. D., Cross, D. J., Minoshima, S., Belongia, D., Watson, G. S., & Craft, S. (2011). Insulin Resistance and Alzheimer-like Reductions in Regional Cerebral Glucose Metabolism for Cognitively Normal Adults With Prediabetes or Early Type 2 Diabetes. *Archives of Neurology*, *68*(1), 71–79. https://doi.org/10.1001/archneurol.2010.225

Belliveau, J., Kennedy, D., McKinstry, R., Buchbinder, B., Weisskoff, R., Cohen, M., … Rosen, B. (1991). Functional mapping of the human visual cortex by magnetic resonance imaging. *Science*, *254*(5032).

Bertoldo, A., Vicini, P., Sambuceti, G., Lammertsma, A. A., Parodi, O., & Cobelli, C. (1998). Evaluation of compartmental and spectral analysis models of [/sup 18/F]FDG kinetics for heart and brain studies with PET. *IEEE Transactions on Biomedical Engineering*, *45*(12), 1429–1448. https://doi.org/10.1109/10.730437

Botkin, C. D., & Osman, M. M. (2007). Prevalence, Challenges, and Solutions for 18F-FDG PET Studies of Obese Patients: A Technologist's Perspective. *Journal of Nuclear Medicine Technology*, *35*(2), 80–83. https://doi.org/10.2967/jnmt.106.034918

Carson, R. E., Channing, M. A., Blasberg, R. G., Dunn, B. B., Cohen, R. M., Rice, K. C., & Herscovitch, P. (1993). Comparison of Bolus and Infusion Methods for Receptor Quantitation: Application to [18 F]Cyclofoxy and Positron Emission Tomography. *Journal of Cerebral Blood Flow & Metabolism*, *13*(1), 24–42. https://doi.org/10.1038/jcbfm.1993.6

Centers for Disease Control and Prevention. (2015, May). About Adult BMI | Healthy Weight | CDC. Retrieved April 21, 2017, from

https://www.cdc.gov/healthyweight/assessing/bmi/adult_bmi/index.html

Chonde, D. B., Izquierdo-Garcia, D., Chen, K., Bowen, S. L., & Catana, C. (2014). Masamune: a tool for automatic dynamic PET data processing, image reconstruction and integrated PET/MRI data analysis. *EJNMMI Physics*, *1*(Suppl 1), A57. https://doi.org/10.1186/2197-7364-1-S1-A57

Cole, E. L., Stewart, M. N., Littich, R., Hoareau, R., & Scott, P. J. H. (2014). Radiosyntheses using fluorine-18: the art and science of late stage fluorination. *Current Topics in Medicinal Chemistry*, *14*(7), 875–900.

Corbetta, M., Miezin, F. M., Dobmeyer, S., Shulman, G. L., & Petersen, S. E. (1990). Attentional Modulation of Neural Processing of Shape, Color, and Velocity in Humans. *Science*, *248*(4962), 1556–1559.

Endo, S., Toyama, H., Kimura, Y., Ishii, K., Senda, M., Kiyosawa, M., & Uchiyama, A. (1997). Mapping visual field with positron emission tomography by mathematical modeling of the retinotopic organization in the calcarine cortex. *IEEE Transactions on Medical Imaging*, *16*(3), 252–260. https://doi.org/10.1109/42.585759

Feng, D., Huang, S.-C., & Wang, X. (1993). Models for computer simulation studies of input functions for tracer kinetic modeling with positron emission tomography. *International Journal of Bio-Medical Computing*, *32*(2), 95–110. https://doi.org/10.1016/0020-7101(93)90049-C

Fischl, B. (2012). FreeSurfer. *NeuroImage*, *62*(2), 774–781. https://doi.org/10.1016/j.neuroimage.2012.01.021

Fox, P. T., Mintun, M. A., Raichle, M. E., Miezin, F. M., Allman, J. M., & Van Essen, D. C. (1986). Mapping human visual cortex with positron emission tomography. *Nature*, *323*(30), 806–809.

Fox, P. T., Mintun, M. A., Reiman, E. M., & Raichle, M. E. (1988). Enhanced Detection of Focal Brain Responses Using Intersubject Averaging and Change-Distribution Analysis of Subtracted PET Images. *Journal of Cerebral Blood Flow & Metabolism*, *8*(5), 642–653. https://doi.org/10.1038/jcbfm.1988.111

Gagnon, L., Sakadžić, S., Lesage, F., Musacchia, J. J., Lefebvre, J., Fang, Q., … Boas, D. A. (2015). Quantifying the microvascular origin of BOLD-fMRI from first principles with two-photon microscopy and an oxygen-sensitive nanoprobe. *The Journal of Neuroscience : The Official Journal of the Society for Neuroscience*, *35*(8), 3663–75. https://doi.org/10.1523/JNEUROSCI.3555-14.2015

Hahn, A., Gryglewski, G., Nics, L., Hienert, M., Rischka, L., Vraka, C., … Lanzenberger, R. (2016). Quantification of Task-Specific Glucose Metabolism with Constant Infusion of 18F-FDG. *Journal of Nuclear Medicine*, *57*(12), 1933–1940. https://doi.org/10.2967/jnumed.116.176156

Hampson, R. E., Porrino, L. J., Opris, I., Stanford, T., & Deadwyler, S. A. (2011). Effects of cocaine rewards on neural representations of cognitive demand in nonhuman primates. *Psychopharmacology*, *213*(1), 105–18. https://doi.org/10.1007/s00213-010-2017-2

Haxby, J. V, Grady, C. L., Horwitz, B., Ungerleider, L. G., Mishkin, M., Carson, R. E., … Rapoport, S. I. (1991). Dissociation of object and spatial visual processing pathways in human extrastriate cortex (regional cerebral blood flow/positron emission tomography). *Neurobiology*, *88*, 1621–1625.

Iozzo, P., Guiducci, L., Guzzardi, M. A., & Pagotto, U. (2012). Brain PET Imaging in Obesity

    and Food Addiction: Current Evidence and Hypothesis. *Obesity Facts*, *5*(2), 155–164.

    https://doi.org/10.1159/000338328

Jones, T., & Rabiner, E. A. (2012). The Development, Past Achievements, and Future Directions

    of Brain PET. *Journal of Cerebral Blood Flow & Metabolism*, *32*(7), 1426–1454.

    https://doi.org/10.1038/jcbfm.2012.20

Jueptner, M., & Weiller, C. (1995). Review: Does Measurement of Regional Cerebral Blood

    Flow Reflect Synaptic Activity?—Implications for PET and fMRI. *NeuroImage*, *2*(2), 148–

    156. https://doi.org/10.1006/nimg.1995.1017

Kalpouzos, G., Eustache, F., Sayette, V., Viader, F., Chételat, G., & Desgranges, B. (2005).

    Working memory and FDG–PET dissociate early and late onset Alzheimer disease patients.

    Journal of Neurology, *252*(5), 548–558. https://doi.org/10.1007/s00415-005-0685-3

Kelloff, G. J. (2005). Progress and Promise of FDG-PET Imaging for Cancer Patient

    Management and Oncologic Drug Development. *Clinical Cancer Research*, *11*(8), 2785–

    2808. https://doi.org/10.1158/1078-0432.CCR-04-2626

Kwong, K. K., Belliveau, J. W., Chesler, D. A., Goldberg, I. E., Weisskoff, R. M., Poncelet, B.

    P., … Rosen, B. R. (1992). Dynamic magnetic resonance imaging of human brain activity

    during primary sensory stimulation. *Neurobiology*, *89*, 5675–5679.

Normandin, M. D., & Morris, E. D. (2008). Estimating neurotransmitter kinetics with ntPET: A

    simulation study of temporal precision and effects of biased data. *NeuroImage*, *39*(3),

    1162–1179. https://doi.org/10.1016/j.neuroimage.2007.09.046

O'Sullivan, F., Kirrane, J., Muzi, M., O'Sullivan, J. N., Spence, A. M., Mankoff, D. A., &

    Krohn, K. A. (2010). Kinetic Quantitation of Cerebral PET-FDG Studies Without

Concurrent Blood Sampling: Statistical Recovery of the Arterial Input Function. *IEEE*

Transactions on Medical Imaging, *29*(3), 610–624.

https://doi.org/10.1109/TMI.2009.2029096

Paulesu, E., Perani, D., Fazio, F., Comi, G., Pozzilli, C., Martinelli, V., … Fieschi, C. (1996).

Functional Basis of Memory Impairment in Multiple Sclerosis: A [18F]FDG PET Study.

NeuroImage, *4*(2), 87–96. https://doi.org/10.1006/nimg.1996.0032

Peirce, J. W. (2007). PsychoPy—Psychophysics software in Python. *Journal of Neuroscience*

Methods, *162*(1–2), 8–13. https://doi.org/10.1016/j.jneumeth.2006.11.017

Peirce, J. W. (2008). Generating stimuli for neuroscience using PsychoPy. *Frontiers in*

Neuroinformatics, *2*. https://doi.org/10.3389/neuro.11.010.2008

Petersen, S. E., Fox, P. T., Posner, M. I., Mintun, M., & Raichle, M. E. (1989). Positron

Emission Tomographic Studies of the Processing of Singe Words. *Journal of Cognitive*

Neuroscience, *1*(2), 153–170. https://doi.org/10.1162/jocn.1989.1.2.153

Pike, G. B. (2012). Quantitative functional MRI: Concepts, issues and future challenges.

NeuroImage, *62*(2), 1234–1240. https://doi.org/10.1016/j.neuroimage.2011.10.046

Placzek, M. S., Zhao, W., Wey, H.-Y., Morin, T. M., & Hooker, J. M. (2016). PET

Neurochemical Imaging Modes. *Seminars in Nuclear Medicine*, *46*(1), 20–27.

https://doi.org/10.1053/j.semnuclmed.2015.09.001

Polimeni, J. R., Fischl, B., Greve, D. N., & Wald, L. L. (2010). Laminar analysis of 7T BOLD

using an imposed spatial activation pattern in human V1. *NeuroImage*, *52*(4), 1334–1346.

https://doi.org/10.1016/j.neuroimage.2010.05.005

Reivich, M., Alavi, A., Wolf, A., Fowler, J., Russell, J., Arnett, C., … Greenberg, J. H. (1985).

Glucose Metabolic Rate Kinetic Model Parameter Determination in Humans: The Lumped

Constants and Rate Constants for [^{18} F]Fluorodeoxyglucose and [^{11} C]Deoxyglucose.

    Journal of Cerebral Blood Flow & Metabolism, *5*(2), 179–192.

    https://doi.org/10.1038/jcbfm.1985.24

Reivich, M., Kuhl, D., Wolf, A., Greenberg, J., Phelps, M., Ido, T., … Sokoloff, L. (1979). The

    [18F]fluorodeoxyglucose method for the measurement of local cerebral glucose utilization

    in man. *Circulation Research*, *44*(1), 127–137. https://doi.org/10.1161/01.RES.44.1.127

Ryan, C. M., Freed, M. I., Rood, J. A., Cobitz, A. R., Waterhouse, B. R., & Strachan, M. W. J.

    (2006). Improving Metabolic Control Leads to Better Working Memory in Adults With

    Type 2 Diabetes. *Diabetes Care*, *29*(2).

Sokoloff, L., Reivich, M., Kennedy, C., Rosiers, M. H. Des, Patlak, C. S., Pettigrew, K. D., …

    Shinohara, M. (1977). The [14-C] deoxyglucose method for the measurement of local

    cerebral glucose utilization: theory, procedure, and normal values in the conscious and

    anesthetized albino rat. *Journal of Neurochemistry*, *28*(5), 897–916.

    https://doi.org/10.1111/j.1471-4159.1977.tb10649.x

Teymurazyan, A., Riauka, T., Jans, H.-S., & Robinson, D. (2013). Properties of noise in positron

    emission tomography images reconstructed with filtered-backprojection and row-action

    maximum likelihood algorithm. *Journal of Digital Imaging*, *26*(3), 447–56.

    https://doi.org/10.1007/s10278-012-9511-5

Villien, M., Wey, H.-Y., Mandeville, J. B., Catana, C., Polimeni, J. R., Sander, C. Y., … Hooker,

    J. M. (2014). Dynamic functional imaging of brain glucose utilization using fPET-FDG.

    NeuroImage, *100*, 192–199. https://doi.org/10.1016/j.neuroimage.2014.06.025

Volkow, N. D., Wang, G., Telang, F., Fowler, J. S., Goldstein, R. Z., Alia-Klein, N., … Pradhan,

    K. (2009). Inverse Association Between BMI and Prefrontal Metabolic Activity in Healthy

Adults. *Obesity*, *17*(1), 60–65. https://doi.org/10.1038/oby.2008.469

Wang, G., Volkow, N., Felder, C., Fowler, J., Levy, A., Pappas, N., … Netusil, N. (2002).
Enhanced resting activity of the oral somatosensory cortex in obese subjects. *Neuroreport*,
13(9), 1151–1155.

Wernick, M. N., & Aarsvold, J. N. (Eds.). (2004). Kinetic Modeling in Positron Emission
Tomography. In *Emission Tomography* (pp. 499–540). Elsevier.

Wey, H.-Y., Gilbert, T. M., Zurcher, N. R., She, A., Bhanot, A., Taillon, B. D., … Hooker, J. M.
(2016). Insights into neuroepigenetics through human histone deacetylase PET imaging.
Science Translational Medicine, *8*(351). https://doi.org/10.1126/scitranslmed.aaf7551

Yehuda, R., Harvey, P. D., Golier, J. A., Newmark, R. E., Bowie, C. R., Wohltmann, J. J., …
Buchsbaum, M. S. (2009). Changes in Relative Glucose Metabolic Rate Following Cortisol
Administration in Aging Veterans with Posttraumatic Stress Disorder: An FDG-PET
Neuroimaging Study. *The Journal of Neuropsychiatry and Clinical Neurosciences*, *21*(2),
132–143. https://doi.org/10.1176/jnp.2009.21.2.132

Zrinzo, L., Yoshida, F., Hariz, M. I., Thornton, J., Foltynie, T., Yousry, T. A., & Limousin, P.
(2011). Clinical Safety of Brain Magnetic Resonance Imaging with Implanted Deep Brain
Stimulation Hardware: Large Case Series and Review of the Literature. *World
Neurosurgery*, *76*(1), 164–172. https://doi.org/10.1016/j.wneu.2011.02.029

Table 1 Subject Information

Subject	Recruitment	Sex	Age	BMI (kg/m^2)	Baseline Plasma Glucose (mg/dL)	30 min. Plasma Glucose (mg/dL)	60 min. Plasma Glucose (mg/dL)
1	Online Ad	Male	48	31.5	102	86	N/A
2	Online Ad	Male	23	25.9	90	N/A	N/A
3	Online Ad	Male	25	28.9	99	68	94
4	Friend	Male	21	23.1	77	78	78
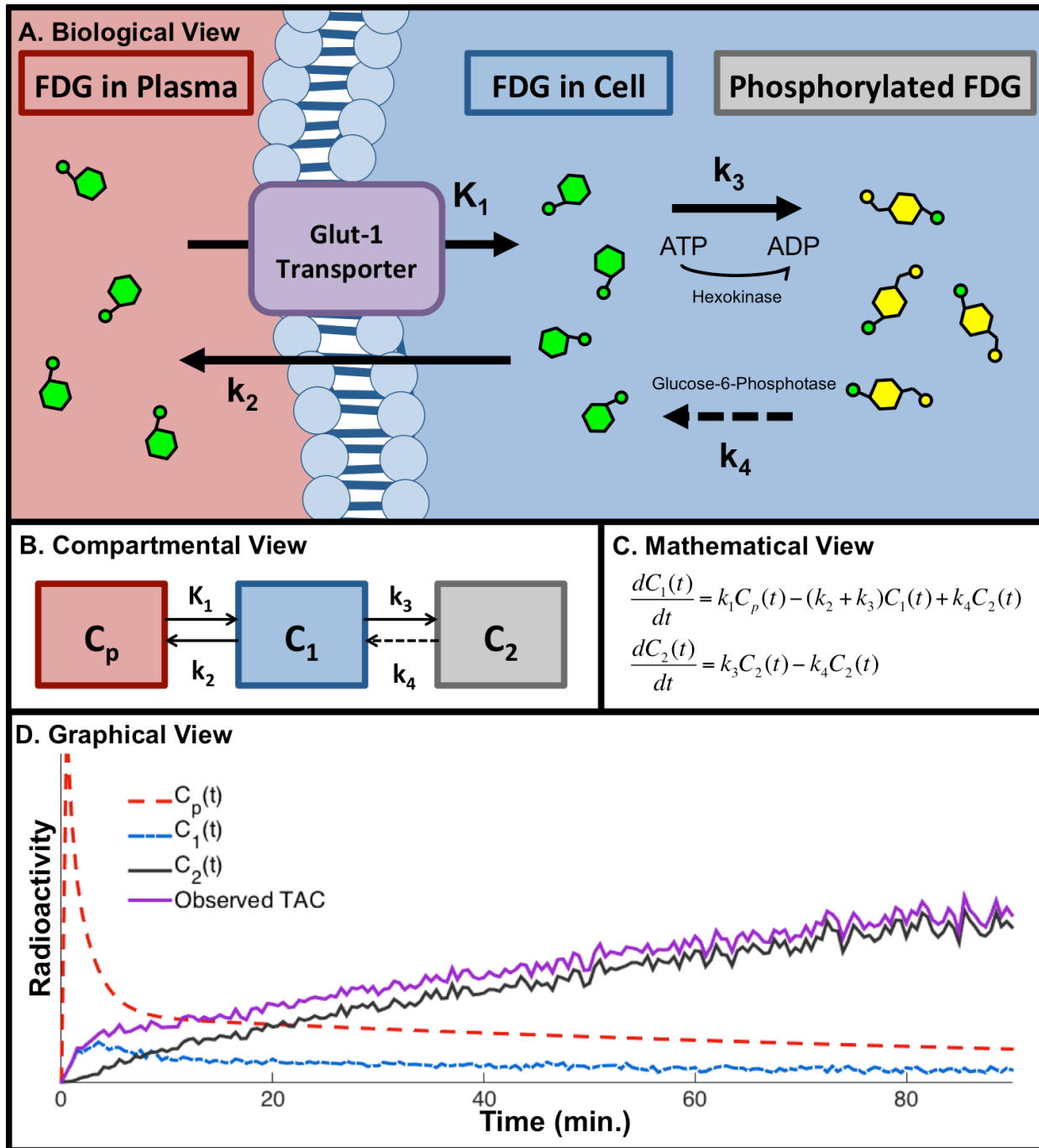
Figure 1 Two-Tissue Compartment Model for FDG

Figure 1. The overall observed signal in FDG-PET is composed of several separate signals. (A) This portion of the figure was adapted from Kelloff et al. (2005). The FDG radiotracer is processed by the body similarly to how glucose is processed. When FDG signal is detected by

the PET scanner, it could have originated from FDG in blood plasma, from FDG that has entered the cell through a Glut-1 transport protein, or from phosphorylated FDG that has begun to undergo the cellular metabolic process of glycolysis. (B) Mathematically, we can predict how much each of these states contributes to the overall FDG signal using a two-tissue compartment (2-TC) model. The compartments C_p, C_1, and C_2 correspond to the amount of FDG that exists in blood plasma, the amount of FDG that has entered the cell, and the amount of FDG that has been phosphorylated, respectively. The parameters K_1, k_2, k_3, and k_4 are rate constants that describe the rate of exchange between compartments. Notably, k_4 is traditionally set to zero or close to zero because very little FDG is ever de-phosphorylated by the enzyme Glucose-6-Phosphotase in the brain. This is represented in the model by a dashed line. (C) The entire 2-TC model can be summarized by a system of differential equations. By providing a plasma input function, $C_p(t)$, and values for the rate constants, $K_1 - k_4$, the system of differential equations can be solved. (D) Solving this system allows us to track the changing concentrations of FDG in each compartment over time. Here, the red line is a simulated plasma input function for a bolus injection of FDG. The blue line represents the changing concentration of FDG in the cell as a result of the plasma input, the black line represents the changing concentration of phosphorylated FDG, and the purple line is an estimate of the overall observed FDG signal.
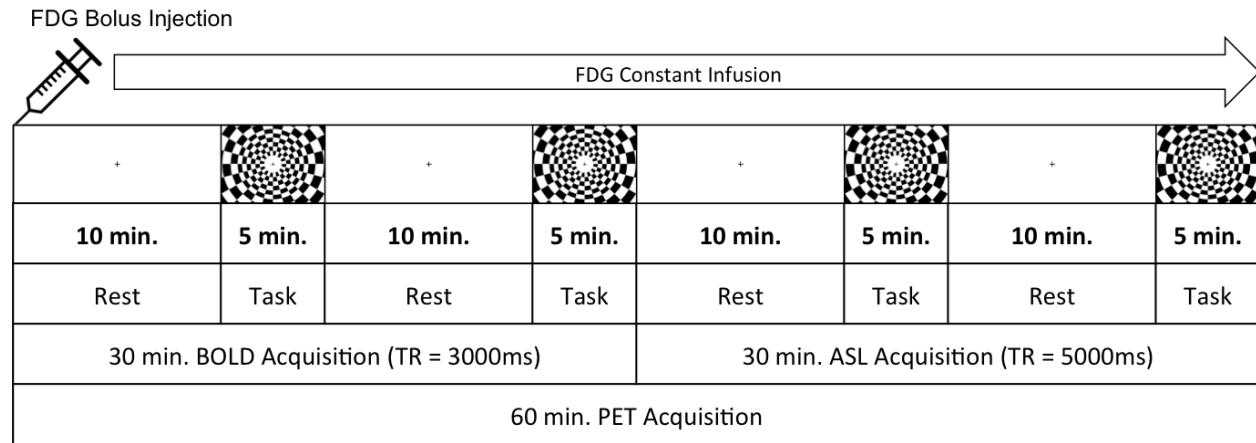
Figure 2 Outline of Experimental Procedure

Figure 2. Participants were scanned using a simultaneous MR/PET scanner for 60 minutes. In the scanner, they alternated viewing a fixation cross on a blank screen (rest period) and a circular flashing checkerboard pattern (task period). Participants received a bolus injection at the start of the scan followed by constant infusion of 2-[^{18}F]-fluorodeoxyglucose (FDG) throughout the entire scan. Dynamic PET images were acquired throughout the entire scan. Simultaneous MRI was acquired as well: BOLD acquisition for the first 30 minutes and arterial spin labeling (ASL) acquisition for the last 30 minutes.
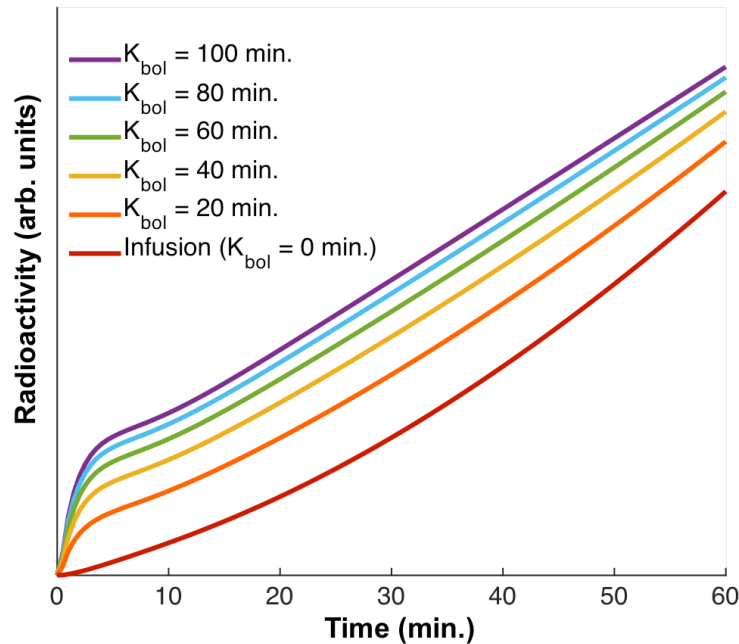
Figure 3 Simulated Tissue Time Activity Curves for Various Values of K_{bol}

Figure 3. K_{bol} is a parameter that summarizes how the dose of a radiotracer is divided between the *initial bolus* and *subsequent constant infusion* in a bolus plus continuous infusion (B/I) protocol. If $K_{bol} = 30$ min., then the bolus portion of the B/I administration is equal in volume to the amount of radiotracer that was constantly infused over 30 minutes. Simulated tissue time activity curves (TAC) are plotted above for various values of K_{bol}. As K_{bol} is increased, a larger portion of the radiotracer dose is injected in the initial bolus, resulting in an overall increase in PET signal. When the radiotracer is constantly infused ($K_{bol} = 0$ min.), it takes about 20-30 minutes before the tissue curve reaches a linear slope (red line). As K_{bol} increases, the tissue TAC reaches a linear slope more quickly. From these simulations, we decided to set $K_{bol} = 60$ min. for the B/I protocol of FDG in this study.
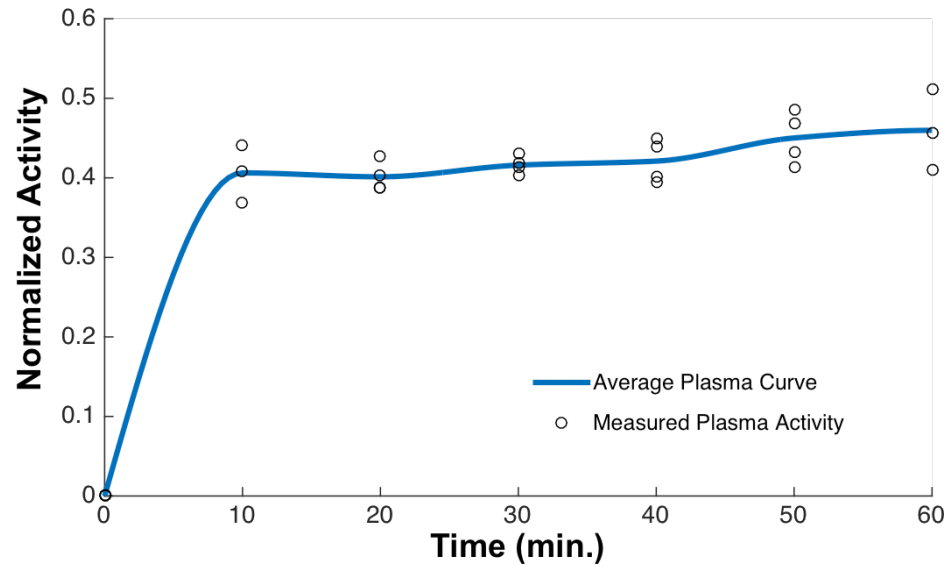
Figure 4 Time Activity Curves for Venous Blood Plasma

Figure 4. Radioactivity in venous plasma was quantified at 10-minute intervals during the scan. Normalized measures for each subject (black circles), along with an interpolated average curve for all subjects (blue line) are presented here. After 10 minutes, a relatively constant value is maintained, confirming that equilibrium was reached in the blood plasma early in the scan.
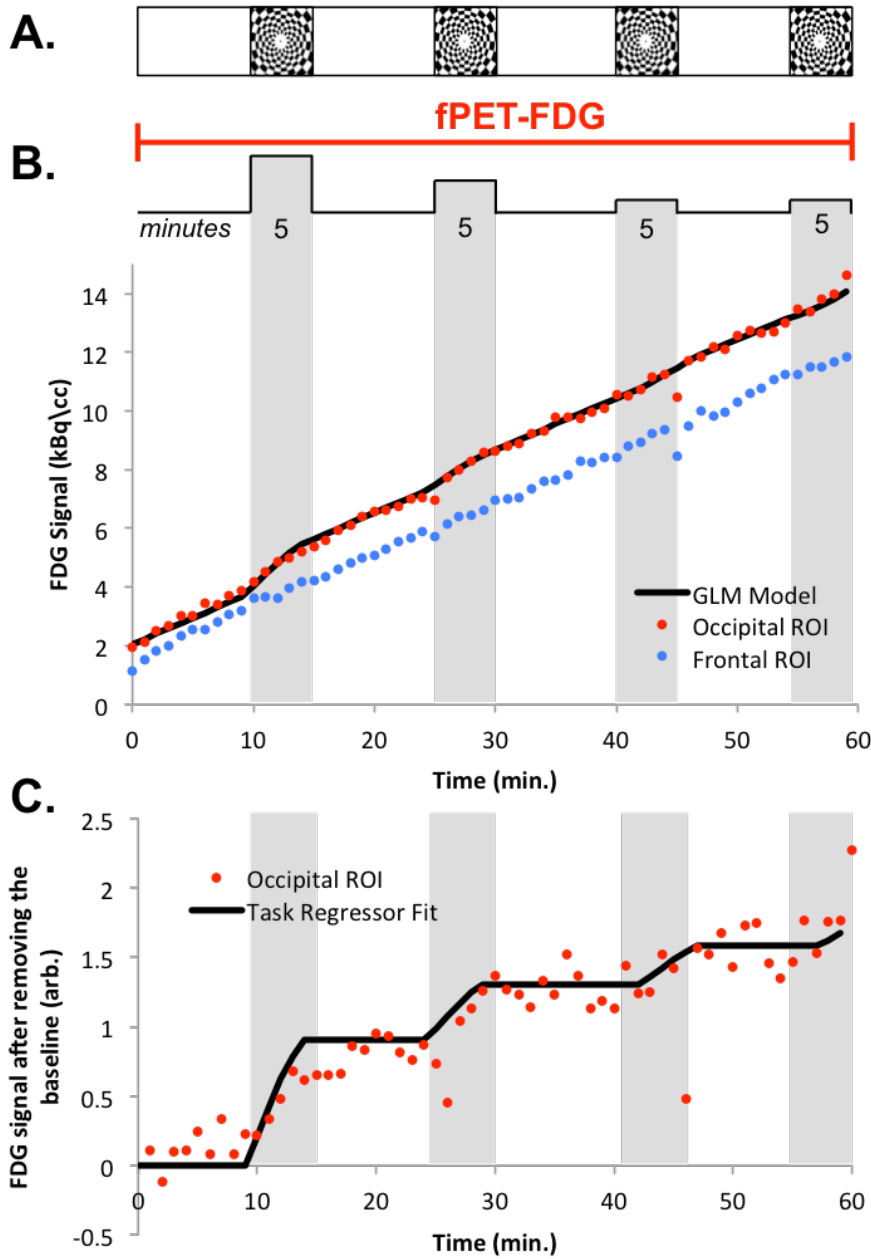
Figure 5 GLM Fit for Subject 4

Figure 5. (A) Subjects in the experiment underwent a 60-minute scan with alternating 10-minute rest periods and 5-minute task periods. During rest periods, subjects viewed a blank white screen with a black fixation cross. During task periods, subjects viewed a flashing circular checkerboard pattern. (B) fPET-FDG signal from manually-drawn regions of interest in the occipital lobe (red) and frontal lobe (blue) are shown. A general linear model (GLM) (black line) was fitted to the

data from the occipital ROI. (C) After subtracting the baseline term of the GLM, the resulting

FDG signal is shown here (red), along with the corresponding task regressor (black line). The

task regressor models increases in the slope of the overall FDG signal that are due solely to the

presentation of the visual stimulus. Data presented in parts B and C of this figure was taken from

subject 4.
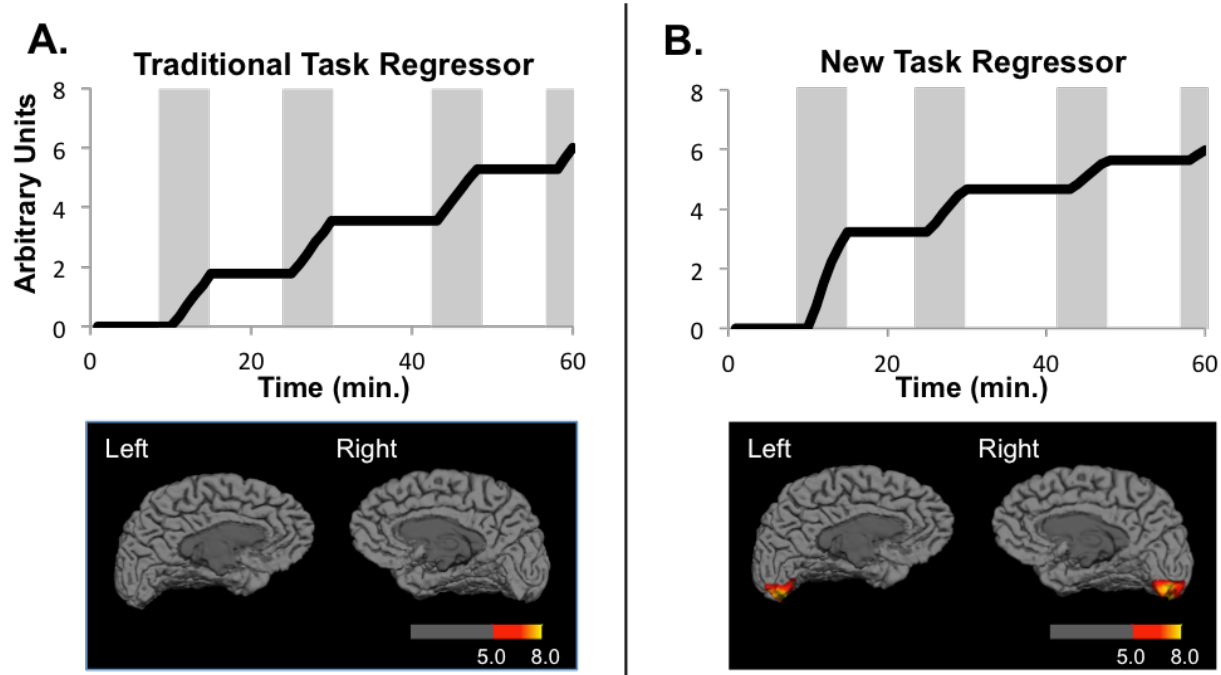
Figure 6 Comparison of Traditional and New General Linear Models in Subject 4

Figure 6. Dynamic PET images from all subjects were analyzed using two general linear models (GLMs). The task regressors from each model predict changes in FDG signal due to the presentation of a flashing checkerboard stimulus at four different times throughout a 60-minute scan. Two possible task-regressors and the resulting statistical maps ($T > 5.0$) are shown for Subject 4. (A) The traditional task regressor predicts that increases in FDG signal would be identical no matter when the stimulus was viewed. A GLM using this regressor does not model the FDG signal in any voxel significantly better than any other voxel, and no activation clusters are observed. (B) A new task regressor predicts that because a bolus plus continuous infusion protocol was used in this study, stimulus-associated increases in FDG signal at the beginning of the scan would be greater than those occurring at later time points. A GLM that uses the new regressor models changes in FDG signal in the subject's occipital lobes significantly better than all other areas of the brain ($T > 5.0$).
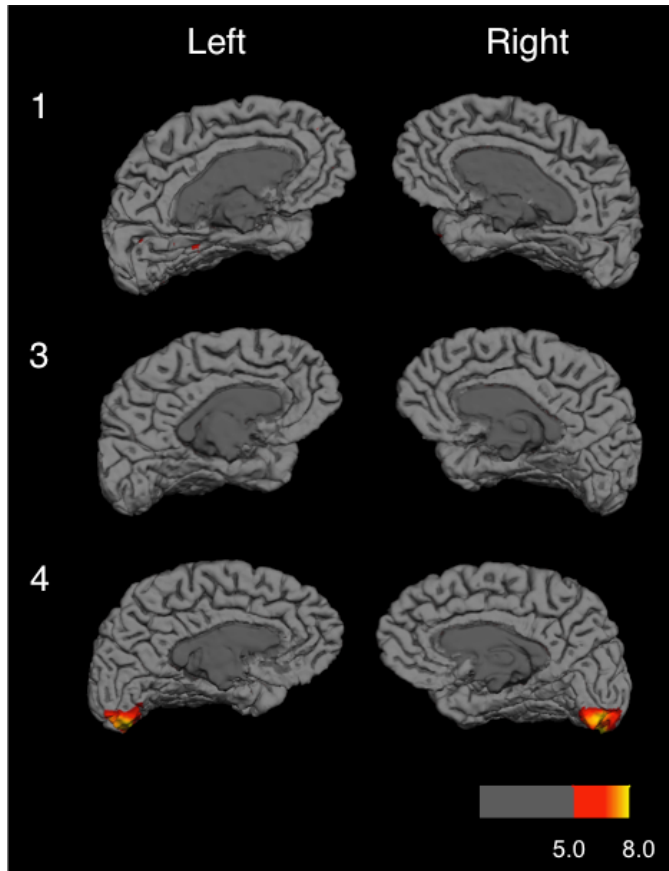
Figure 7 fPET-FDG Activation Maps

Figure 7. Statistical maps ($T > 5.0$) for subjects 1, 3, and 4 highlight brain regions that show increased FDG signal changes during the display of a flashing circular checkerboard pattern. Subject 2 was excluded from this analysis because he exhibited significant head motion during the scan (> 5mm). Subjects 1 and 3 do not show any significant regions of activation. Subject 4 shows bilateral activation in area V1 of the occipital lobe.
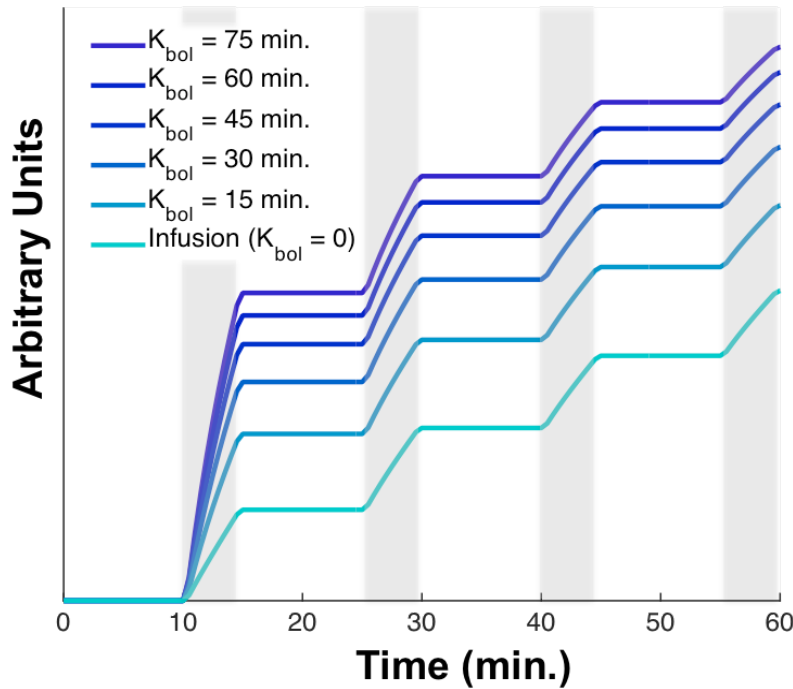
Figure 8. Task Regressors for Various K_{bol} Values

Figure 8. Task regressors predict the magnitude of task-associated changes in FDG signal over a 60-minute scan. Four simulated task-periods are shaded in gray. For a constant infusion protocol ($K_{bol} = 0$ min.), the regressor predicts that all task-associated changes in FDG signal will be of equal magnitude, no matter when the tasks occur during the scan. For bolus plus continuous infusion protocols with higher values of K_{bol}, the corresponding task regressors predict that earlier task-periods will result in greater FDG signal changes than later task-periods.

Appendix

Here, we derive our equation for generating a simulated bolus plus continuous infusion protocol from the method proposed by Carson, et al. (1993). Carson, et al. present the following method for deriving the equivalent bolus infusion protocol $H(t)$ from a bolus previously known bolus protocol $f(t)$:

$$H(t) = \frac{K_{bol}\delta(t) + \theta(t) - \theta(t - T)}{K_{bol} + T} \text{ where } \theta(t) = \begin{cases} 0, & t < 0 \\ 1, & t > 0 \end{cases}$$

$T = $ the duration of the scan and $\delta(t)$ is the Dirac delta function

$$g(t) = H(t) \otimes f(t)$$

$$= \frac{K_{bol} f(t) + \int_0^t f(\tau)d\tau}{K_{bol} + T}$$

$$= \frac{K_{bol} f(t)}{K_{bol} + T} + \frac{(T) \int_0^t f(\tau)d\tau}{T (K_{bol} + T)}$$

$$= \frac{K_{bol} f(t)}{K_{bol} + T} + \frac{(K_{bol} - K_{bol} + T) \int_0^t f(\tau)d\tau}{T(K_{bol} + T)}$$

$$= \frac{K_{bol} f(t)}{K_{bol} + T} + \left(\frac{K_{bol} + T}{K_{bol} + T} - \frac{K_{bol} \int_0^t f(\tau)d\tau}{T(K_{bol} + T)} \right)$$

$$= R_{bol} f(t) + \left(1 - R_{bol} \frac{\int_0^t (\tau)d\tau}{T} \right) \text{ where } R_{bol} = \frac{K_{bol}}{K_{bol} + T}$$

$$= R_{bol} f(t) + R_{inf} \frac{\int_0^t f(\tau)d\tau}{T} \text{ where } R_{inf} = 1 - R_{bol}$$

Therefore, we can use the equation $g(t) = R_{bol} f(t) + R_{inf} \frac{\int_0^t f(\tau)d\tau}{T}$ to map a known bolus curve f(t) to an equivalent bolus plus continuous infusion curve g(t), give the ration of bolus to infusion $R_{bol} = \frac{K_{bol}}{K_{bol} + T}$.